Magnetic control of ferroelectric polarization

T. Kimura[1]*, T. Goto[1], H. Shintani[1], K. Ishizaka[1], T. Arima[2] & Y. Tokura[1]

[1]*Department of Applied Physics, University of Tokyo, Tokyo 113-8656, Japan*
[2]*Institute of Materials Science, University of Tsukuba, Tsukuba 305-8573, Japan*

* Present address: Los Alamos National Laboratory, Los Alamos, New Mexico 87545, USA

The magnetoelectric effect—the induction of magnetization by means of an electric field and induction of polarization by means of a magnetic field—was first presumed to exist by Pierre Curie[1], and subsequently attracted a great deal of interest in the 1960s and 1970s (refs 2–4). More recently, related studies on magnetic ferroelectrics[5–14] have signalled a revival of interest in this phenomenon. From a technological point of view, the mutual control of electric and magnetic properties is an attractive possibility[15], but the number of candidate materials is limited and the effects are typically too small to be useful in applications. Here we report the discovery of ferroelectricity in a perovskite manganite, $TbMnO_3$, where the effect of spin frustration causes sinusoidal antiferromagnetic ordering. The modulated magnetic structure is accompanied by a magnetoelastically induced lattice modulation, and with the emergence of a spontaneous polarization. In the magnetic ferroelectric $TbMnO_3$, we found gigantic magnetoelectric and magnetocapacitance effects, which can be attributed to switching of the electric polarization induced by magnetic fields. Frustrated spin systems therefore provide a new area to search for magnetoelectric media.

The room-temperature crystal structure of $TbMnO_3$ investigated here is the orthorhombically distorted perovskite structure (space group *Pbnm*; Fig. 1a). We note that the perovskite structure of $TbMnO_3$ is distinct from that of the antiferromagnetic (AF) ferroelectric hexagonal rare-earth manganites (for example, $YMnO_3$) in which magnetoelectric coupling has been well studied[5–9]. Furthermore, the perovskite $TbMnO_3$ does not contain 6*s* lone pairs, which produce a polar structure in magnetic ferroelectric perovskites $BiMnO_3$ (refs 11–13) and $BiFeO_3$ (ref. 14). The electronic configuration of the Mn^{3+} site in $TbMnO_3$ is identical with that in the parent compound of colossal magnetoresistive manganites, $LaMnO_3$, having the $t_{2g}^3 e_g^1$ configuration. In $LaMnO_3$, staggered orbital order of the $d_{3x^2-r^2}/d_{3y^2-r^2}$ type is responsible for the layered (A-type) AF order. In contrast, the spin structure in $TbMnO_3$ is a sinusoidal AF ordering of the Mn^{3+} moments that takes place at

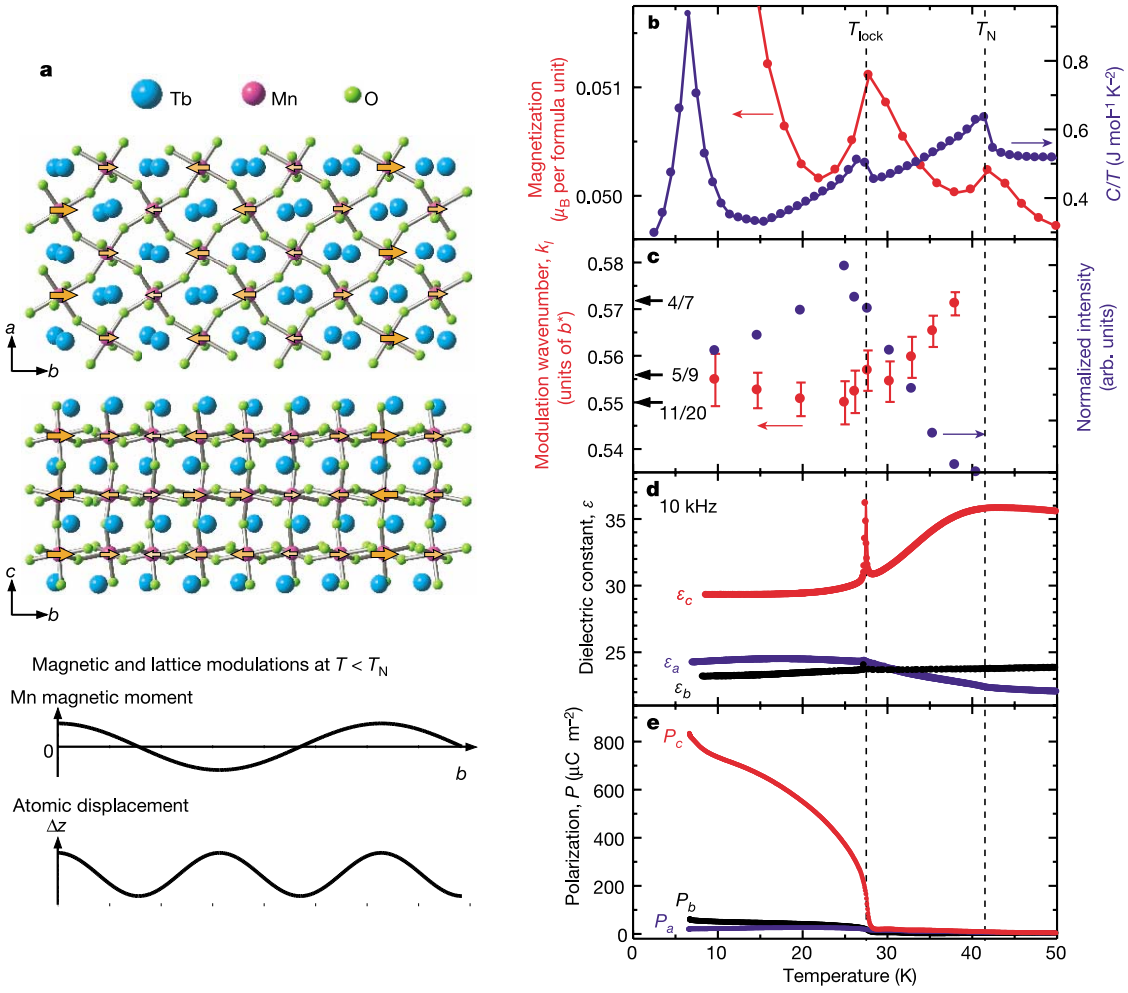

Figure 1 Appearance of ferroelectricity below a lock-in transition temperature in $TbMnO_3$. **a**, Rough sketches of crystal structure at room temperature (top) and spatial variation along the *b* axis of Mn magnetic moment and atomic displacement ($\Delta z//c$) below T_N (lower). Orange arrows denote Mn magnetic moments below T_N. **b**–**e**, Temperature profiles of magnetization and specific heat divided by temperature C/T (**b**), wavenumber of lattice modulation k_l (**c**), dielectric constant ϵ at 10 kHz (**d**), and electric polarization P along the principal axes in single crystals of $TbMnO_3$ (**e**). The error bars of k_l denote the distribution of k related to the correlation length.

$T_N \approx 41$ K with a wave vector $\mathbf{q} = (0,k_s,1)$ in the *Pbnm* orthorhombic cell[16]. A Mn^{3+} moment oriented along the *b* axis has been proposed[16]. The wavenumber k_s is incommensurate ($\sim$0.295) at T_N and decreases with decreasing temperature, becoming nearly constant (0.28) below $\sim$30 K. A rough sketch of the magnetic order on Mn moments is illustrated in Fig. 1a. Recently, the emergence of long-period sinusoidal AF order in $TbMnO_3$ has been explained in terms of spin frustration caused by the combination of a $GdFeO_3$-type distortion and staggered orbital order[17].

We show in Fig. 1b temperature (T) profiles of magnetization (M) at 0.5 T, and of specific heat divided by temperature (C/T), for a single crystal of $TbMnO_3$. Both M and C/T exhibit three anomalies at $\sim$7 K, $\sim$27 K and $\sim$42 K. Taking account of results of a former neutron diffraction study[16], the anomalies at $\sim$7 K and $\sim$42 K are attributed to the magnetic ordering of the Tb^{3+} moments and the sine-wave ordering of the Mn^{3+} moments, respectively. The anomaly at 27 K seems to be related to the incommensurate–commensurate (or lock-in) transition where the magnetic modulation wave vector $\mathbf{k}_s$ is locked at a constant value.

X-ray diffraction measurements revealed that the modulated magnetic ordered phase is accompanied by magnetoelastically induced lattice modulation[17]. Figure 1c displays the T dependence of wavenumber k_l and normalized intensity of a superlattice reflection at $(0,k_l,3)$ attributed to the lattice modulation. The superlattice reflections at the wave vector $(0,k_l,l)$ with l an integer, appear below $T_N \approx 41$ K ($k_l \approx 0.57$ at T_N). The intensity of the superlattice reflections increases down to the lock-in transition temperature ($T_{lock} \approx 27$ K), but is suppressed again below T_{lock}. Another notable feature is the T dependence of the modulation wavenumber k_l, as clarified in Fig. 1c. Upon cooling from T_N down to T_{lock}, k_l decreases and then becomes nearly constant ($k_l \approx 0.55$) below T_{lock}. The value of the T-dependent k_l is almost twice as large as that of the magnetic wavenumber k_s (ref. 16). It is well known that the crystallographic deformations upon magnetic ordering are caused by the magnetic atoms increasing their exchange interaction energy by shifting their positions; that is, exchange striction[18,19]. By analogy with the lattice modulations observed in some rare-earth metals such as Tm with sinusoidal order[20,21], the observed superlattice reflections due to atomic displacement can be regarded as a second harmonic that is magnetoelastically induced by sinusoidal AF order.

In materials with incommensurate phases[22], such as the family of A_2BX_4 compounds (for example, Rb_2ZnCl_4, $(NH_4)_2BeF_4$ and K_2SeO_4), the lattice modulation is generally connected with a spatially varying electric polarization. With further decreasing temperature, these materials exhibit a first-order phase transition (lock-in transition) to a ferroelectric phase with finite spontaneous polarization. Taking account of these observations, we could expect to find ferroelectricity in $TbMnO_3$ associated with the incommensurate phase at the lock-in transition. Thus, we performed measurements of the dielectric constant, ϵ, and the electric polarization, P, along the *a*, *b* and *c* axes. Figure 1d displays T profiles of ϵ at 10 kHz. While ϵ_b (electric field E parallel to the *b* axis; $E\|b$) shows merely weak T dependence, several anomalies are observed in ϵ_a ($E\|a$) and ϵ_c ($E\|c$). ϵ_a increases below $T_N \approx 41$ K towards low temperature, and becomes nearly constant below T_{lock}. The most striking feature is observed in ϵ_c. A pronounced λ-type peak of ϵ_c is found at T_{lock}, although no distinct anomaly is observed at T_N. The sharp peak structure in ϵ_c at T_{lock} is suggestive of the occurrence of the ferroelectric phase transition. To confirm the ferroelectric activity, we show in Fig. 1e the temperature variation of P. A finite spontaneous polarization appears below T_{lock} along the *c* axis. P_c ($P\|c$) at $\sim$10 K is about 8×10^{-4} C m^{-2}. We also confirmed that P_c can be reversed by the d.c. electric field. Thus, $TbMnO_3$ becomes ferroelectric below T_{lock}.

The spontaneous polarization of $TbMnO_3$ is rather small compared with that of conventional ferroelectrics (for example, $\sim 2.6 \times 10^{-2}$ C m^{-2} at 296 K in $BaTiO_3$), but is comparable to that of the so-called improper ferroelectrics[23] (for example, $\sim 1.2 \times 10^{-3}$ C m^{-2} at 153 K in Rb_2ZnCl_4 (ref. 24) and $\sim 5.6 \times 10^{-4}$ C m^{-2} at 77 K in K_2SeO_4 (ref. 25)). In improper ferroelectrics, the primary order parameter represents the lattice distortion mode having a nonzero wave vector (that is $k_l \neq 0$), and the spontaneous polarization appears as a secondary order parameter induced by the lattice distortion. This may also be the case for $TbMnO_3$. An uncompensated antidipole structure is possible in

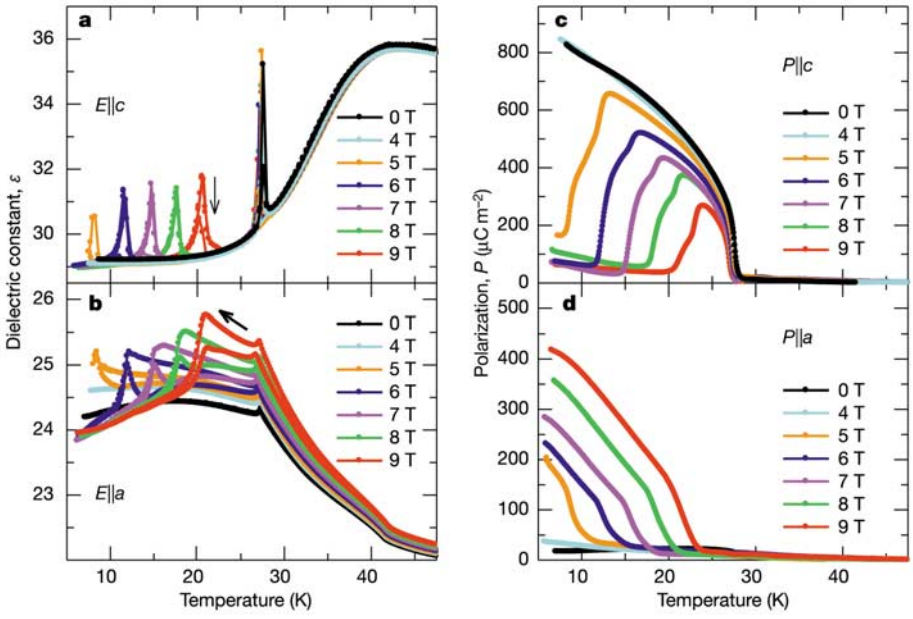

Figure 2 Electric polarization flop induced by magnetic fields in $TbMnO_3$. **a**–**d**, Temperature profiles of dielectric constant at 10 kHz (**a** and **b**) and of electric polarization along the *c* and *a* axes (**c** and **d**), respectively, at various magnetic fields in single crystals of $TbMnO_3$. Magnetic fields are applied along the *b* axis.

improper ferroelectrics, which was specified by the term ferrielectricity[26] because of its analogy with ferrimagnetism. Indeed, the intensity comparison of the superlattice reflections at $(0,k_l,0)$ and $(0,k_l,2)$ measured by the X-ray diffraction suggests that the atomic displacement in the ferroelectric phase has a component along the c axis, that is, the direction of the spontaneous polarization (Fig. 1a). In addition, weak intensities of the superlattice reflections (five orders of magnitude smaller than the Bragg peak) and the lack of their enhancement on tuning the X-ray photon energy at Mn K- and Tb L-absorption edges suggest the lattice distortion is due to the displacement of O ions.

As the lattice modulation in $TbMnO_3$ is accompanied by magnetic order, we may expect coupling between magnetization and polarization. We have investigated the effect of magnetic field on ϵ and P. In the experiments, magnetic fields (B) were applied along the b axis, that is, the direction of the modulation wave vector and the Mn^{3+} magnetic moments. Figure 2a and b shows the T profiles of ϵ along the c and a axes, respectively, at various magnetic fields. No distinct change of ϵ for either direction was observed at temperatures above T_{lock}. Although the sharp peak at T_{lock} in ϵ_c is not sensitive to the application of magnetic fields, another peak feature at $T_{flop}(B)$ shows up in ϵ_c below T_{lock} above 5 T. The magnetic-field-induced sharp maximum is shifted towards higher T with increasing magnetic field from $T_{flop}(5\,T) \approx 8$ K to $T_{flop}(9\,T) \approx 20$ K. The component ϵ_a also shows a remarkable magnetic field effect. By applying magnetic fields above 5 T, ϵ_a exhibits a peak structure at T_{flop}, and shows a thermal hysteresis at a temperature between T_{flop} and T_{lock}. We also measured the ϵ_b in magnetic fields, but no substantial magnetic field effect was observed up to 9 T.

Measurements of P in magnetic fields have revealed the origin of the magnetic-field-induced anomaly in ϵ. We show in Fig. 2c and d the T variation of P_c and P_a, respectively, at various magnetic fields. By applying a magnetic field above ~5 T, the spontaneous polarization in P_c is considerably suppressed below T_{flop}. With increasing magnetic field, the temperature region with finite P_c shrinks, corresponding to the shift of T_{flop}. By contrast, the application of a magnetic field induces a finite P_a (Fig. 2d). The onset temperature of a finite P_a coincides well with T_{flop}, and increases in accord with the increase of T_{flop} by applying a magnetic field. These results show that the spontaneous polarization is switched ('flopped') from the direction along the c axis to the direction along the a axis at T_{flop}, and the strong magnetic field dependence of T_{flop} causes the notable magnetic field effect on ϵ and P.

We display in Fig. 3 the magnetic field dependence of the change in ϵ ($\Delta\epsilon(B)/\epsilon(0) = [\epsilon(B) - \epsilon(0)]/\epsilon(0)$), P and magnetization at selected temperatures. As shown in Fig. 3a and b, a remarkable

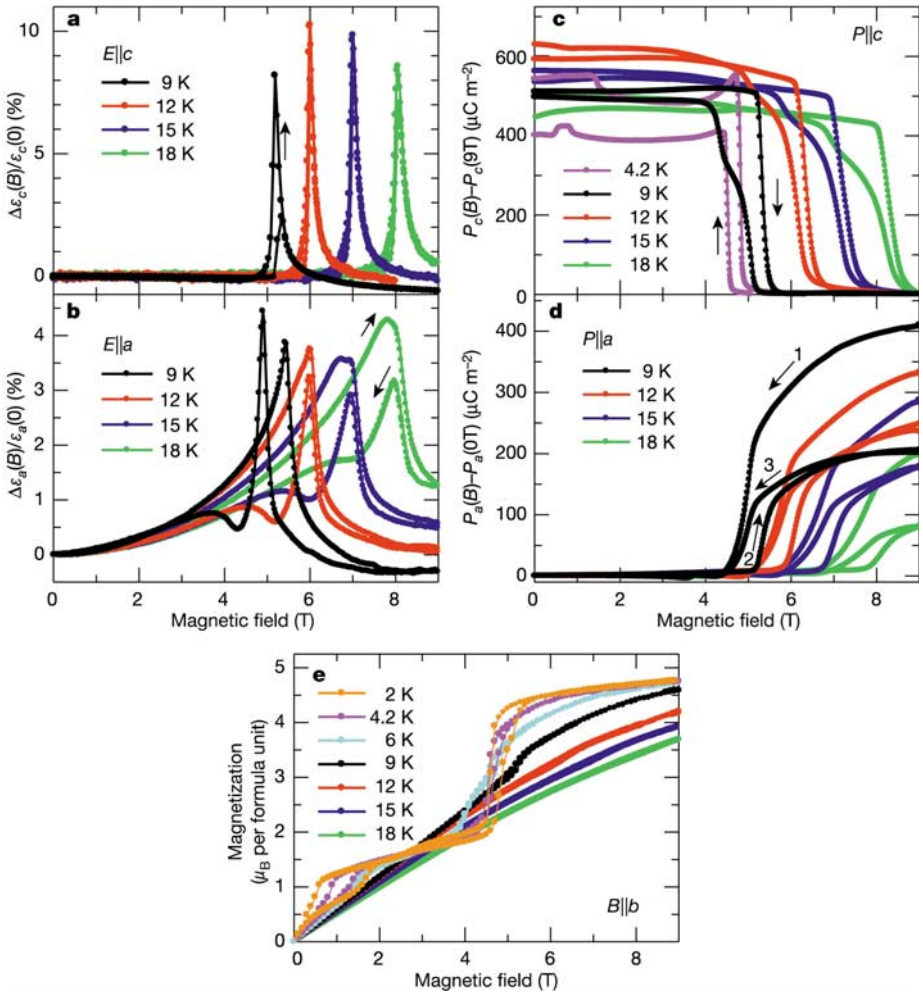

Figure 3 Magnetocapacitance and magnetoelectric effects in $TbMnO_3$. **a**–**e**, Magnetic-field-induced change in dielectric constant (**a** and **b**), electric polarization along the c and a axes, respectively (**c** and **d**), and magnetization at selected temperatures (**e**). Magnetic fields are applied along the b axis. The magnetic field dependence of electric polarization was obtained by the measurements of magnetoelectric current, which were performed after poling crystals. The data of **d** were collected after the magnetic field cooling. The numbers in **d** denote the order of measurements at 9 K.

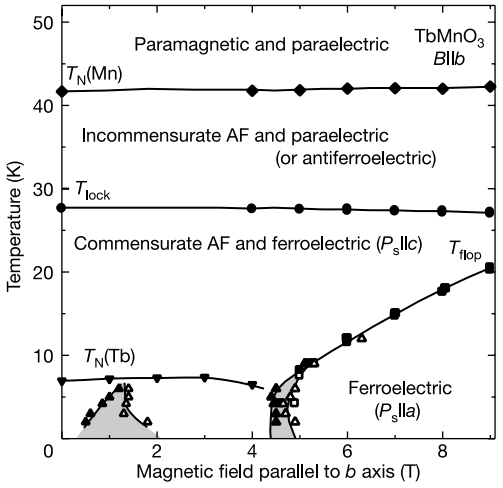

Figure 4 Temperature versus magnetic field phase diagram for $TbMnO_3$ for magnetic field applied along the *b* axis. Open and filled symbols represent the data points in the cooling (or magnetic-field increasing) and warming (or magnetic-field decreasing) runs, respectively. T_N(Mn) (determined from the dielectric anomaly in ϵ_a) and T_N(Tb) (determined from the anomaly in the *M*–*T* curve) indicate the antiferromagnetic ordering temperature of the Mn^{3+} and Tb^{3+} moments, respectively. T_{lock} and T_{flop}, which were determined from the dielectric anomaly, denote the temperatures of incommensurate–commensurate (or lock-in) transition and electric polarization flop, respectively. Triangles indicate the points where the magnetization curves show steep steps. The shaded areas show magnetic field hysteresis regions.

peak structure with hysteresis is observed at almost the same magnetic field for both $\Delta\epsilon_c(B)/\epsilon_c(0)$ and $\Delta\epsilon_a(B)/\epsilon_a(0)$ at their respective temperatures. The peak position $B_{flop}(T)$ is shifted towards higher magnetic field with increasing temperature. The maximum value of the magnetocapacitance as defined by $\Delta\epsilon(B_{flop})/\epsilon(0)$ reaches values as large as ~10% at 12 K. The divergent increase of ϵ at B_{flop} has an intimate connection to the magnetic-field-induced electric polarization flop, which is confirmed by the magnetic field dependence of *P* (Fig. 3c and d). The spontaneous polarization along the *c* axis is suddenly suppressed at B_{flop}, whereas that along the *a* axis appears at B_{flop} with increasing magnetic fields. The data in Fig. 3c and d can be regarded as a novel magnetoelectric effect, where the gigantic change in P ($\Delta P(B) \approx 6 \times 10^{-4}\,C\,m^{-2}$) is caused by the magnetic-field-induced electric polarization flop with the nature of first-order phase transition.

To sum up the present study, we have determined the electric and magnetic phase diagram of $TbMnO_3$ from dielectric and magnetic anomalies for the direction of magnetic field parallel to the *b* axis (Fig. 4). The magnetic phase boundaries denoted by triangles are determined from steep steps in magnetization curves (Fig. 3e). This clearly indicates that $T_{flop}(B)$ is in good agreement with a magnetic phase boundary. Similar metamagnetic transitions also take place in a rare-earth orthoferrite, $TbFeO_3$, and this has been interpreted as the magnetic reversal of Ising Tb^{3+} moments[27,28]. Furthermore, the Tb^{3+} spin reversal gives rise to the spin reorientation in Fe sites. By analogy, it is likely in the magnetic-field-induced electric polarization flop of $TbMnO_3$ that Tb^{3+} moment reversal, accompanied by the Mn spin reorientation, changes the exchange interaction energy and then brings about the lattice modulation owing to a finite spontaneous polarization along the *a* axis. The giant magnetocapacitance and magnetoelectric effects as observed in the present frustrated-spin system may provide intriguing opportunities to explore a new type of magnetoelectric functionality. □

Methods

Single crystals of $TbMnO_3$ were grown in a flow of Ar by the floating zone method. The crystals were oriented using Laue X-ray diffraction patterns, and cut into thin plates (typical dimensions, $\sim 3 \times 3 \times 1\,mm^3$) with the widest faces perpendicular to the crystallographic principal axes. The magnetization and specific heat for the crystals were measured with a commercial magnetometer and a relaxation technique, respectively. Single-crystal diffraction measurements were performed at BL-4C of the Photon Factory, KEK, in Tsukuba. X-rays with photon energy of 13 keV were used for the non-resonant X-ray scattering, and that near the Mn *K*- and Tb *L*-absorption edges for the resonant one. The dielectric constant was measured at 10 kHz using an LCR meter. The *T* dependence of electric polarization was obtained by measurements of pyroelectric current. The sample was cooled down while applying a poling field ($\sim 150\,kV\,m^{-1}$). At the lowest *T*, the poling electric field was removed. Then, the sample was heated at a constant rate ($5\,K\,min^{-1}$), and the pyroelectric current was measured. For these electric measurements, silver electrodes were evaporated onto the widest faces of the sample.

Received 26 May; accepted 26 August 2003; doi:10.1038/nature02018.

1. Curie, P. Sur la symétrie dans les phénomenes physiques, symétrie d'un champ électrique et d'un champ magnétique. *J. Phys.* **3** (Ser. III), 393–415 (1894).
2. O'Dell,, T. H. *The Electrodynamics of Magneto-Electric Media* (North-Holland, Amsterdam, 1970).
3. Freeman, A. J. & Schmid, H. (eds) *Magnetoelectric Interaction Phenomena in Crystals* (Gordon and Breach, London, 1975).
4. Smolenskii, G. A. & Chupis, I. E. Ferroelectromagnets. *Usp. Fiz. Nauk.* **137,** 415–448 (1982); also *Sov. Phys. Usp.* **25,** 475–493 (1982).
5. Huang, Z. J., Cao, Y., Sun, Y., Xue, Y. Y. & Chu, C. W. Coupling between the ferroelectric and antiferromagnetic orders in $YMnO_3$. *Phys. Rev. B* **56,** 2623–2626 (1997).
6. Iwata, N. & Kohn, K. Dielectric anomalies at magnetic transitions of hexagonal rare earth manganese oxides $RMnO_3$. *J. Phys. Soc. Jpn* **67,** 3318–3319 (1998).
7. Katsufuji, T. *et al.* Dielectric and magnetic anomalies and spin frustration in hexagonal $RMnO_3$ (R = Y, Yb, and Lu). *Phys. Rev. B* **64,** 104419 (2001).
8. Fiebig, M., Lottermoser, Th., Fröhlich, D., Goltsev, A. V. & Pisarev, R. V. Observation of coupled magnetic and electric domains. *Nature* **419,** 818–820 (2002).
9. Hanamura, E., Hagita, K. & Tanabe, Y. Clamping of ferroelectric and antiferromagnetic order parameters of $YMnO_3$. *J. Phys. Condens. Matter* **14,** L103–L109 (2003).
10. Zhong, C. G. & Jiang, Q. The study of the coupling mechanism between antiferromagnetic and ferroelectric ordering and thermodynamic properties in ferroelectromagnets. *J. Phys. Condens. Matter* **14,** 8605–8612 (2002).
11. Seshadri, R. & Hill, N. A. Visualizing the role of Bi 6s "lone pairs" in the off-center distortion in ferromagnetic $BiMnO_3$. *Chem. Mater.* **13,** 2892–2899 (2001).
12. Moreira dos Santos, A. *et al.* Evidence for the likely occurrence of magnetoferroelectricity in the simple perovskite, $BiMnO_3$. *Solid State Commun.* **122,** 49–52 (2002).
13. Kimura, T. *et al.* Magnetocapacitance effect in multiferroic $BiMnO_3$. *Phys. Rev. B* **67,** 180401(R) (2003).
14. Wang, J. *et al.* Epitaxial $BiFeO_3$ multiferroic thin film heterostructures. *Science* **299,** 1719–1722 (2003).
15. Wood, V. E. & Austin, A. E. Possible applications for magnetoelectric materials. *Int. J. Magn.* **5,** 303–315 (1974).
16. Quezel, S., Tcheou, F., Rossat-Mignod, J., Quezel, G. & Roudaut, E. Magnetic structure of the perovskite-like compound $TbMnO_3$. *Physica B* **86–88,** 916–918 (1977).
17. Kimura, T. *et al.* Distorted perovskite with e_g^1 configuration as a frustrated spin system. *Phys. Rev. B* **68,** 060403(R) (2003).
18. Greenwald, S. & Smart, J. S. Deformations in the crystal structures of anti-ferromagnetic compounds. *Nature* **166,** 523–524 (1950).
19. Smart, J. S. & Greenwald, S. Crystal structure transitions in antiferromagnetic compounds at the Curie temperature. *Phys. Rev.* **82,** 113–114 (1951).
20. Bohr, J. *et al.* Diffraction studies of rare earth metals and superlattices. *Physica B* **159,** 93–105 (1989).
21. Bohr, J., Gibbs, D. & Huang, K. X-ray-diffraction studies of the magnetic state of thulium. *Phys. Rev. B* **42,** 4322–4328 (1990).
22. Blinc, R. & Levanyuk, A. P. *Incommensurate Phases in Dielectrics 1. Fundamentals* (North-Holland, Amsterdam, 1986).
23. Levanyuk, A. P. & Sannikov, D. G. Improper ferroelectrics. *Usp. Fiz. Nauk.* **112,** 561–589 (1974); also *Sov. Phys. Usp.* **17,** 199–214 (1974).
24. Sawada, S., Shiroishi, Y., Yamamoto, A., Takashige, M. & Matsuo, M. Ferroelectricity in Rb_2ZnCl_4. *J. Phys. Soc. Jpn* **43,** 2099–2100 (1977).
25. Aiki, K., Hukuda, K. & Matumura, O. Ferroelectricity in K_2SeO_4. *J. Phys. Soc. Jpn* **26,** 1064 (1969).
26. Goldsmith, G. J. & White, J. G. Ferroelectric behavior in thiourea. *J. Chem. Phys.* **31,** 1175–1187 (1959).
27. Bouree, J. E. & Hammann, J. Mise en évidence expérimentale des effets de forme dans l'orthoferrite de terbium. *J. Phys.* **36,** 391–397 (1975).
28. Bidaux, R., Bouree, J. E. & Hammann, J. Diagramme de phase de l'orthoferrite de terbium en présence d'un champ magnétique. *J. Phys.* **36,** 803–809 (1975).

Acknowledgements We thank K. Kohn, K. Ohgushi, S. Ishihara and A. P. Ramirez for discussions, and Y. Wakabayashi for help with X-ray diffraction measurements. This work was partly supported by KAKENHI from the MEXT of Japan.

Competing interests statement The authors declare that they have no competing financial interests.

Correspondence and requests for materials should be addressed to T.K. (tkimura@lanl.gov).